

The Origins of I-type Spherules and the Atmospheric Entry of Iron Micrometeoroids.

Matthew J. Genge

Impact and Astromaterials Research Centre (IARC), Department of Earth Science and Engineering, Imperial College London, Exhibition Road, London SW7 2AZ, UK & Department of Mineralogy, The Natural History Museum, Cromwell Road, London SW7 2BT. email: m.genge@imperial.ac.uk

ABSTRACT

The Earth's extraterrestrial dust flux includes a wide variety of dust particles that include FeNi metallic grains. During their atmospheric entry iron micrometeoroids melt and oxidize to form cosmic spherules termed I-type spherules. These particles are chemically resistant and readily collected by magnetic separation and are thus the most likely micrometeorites to be recovered from modern and ancient sediments. Understanding their behavior during atmospheric entry is crucial in constraining their abundance relative to other particle types and the nature of the zodiacal dust population at 1 AU. This paper presents numerical simulations of the atmospheric entry heating of iron meteoroids in order to investigate the abundance and nature of these materials. The results indicate that iron micrometeoroids experience peak temperatures 300-800K higher than silicate particles explaining the rarity of unmelted iron particles which can only be present at sizes of $<50 \mu\text{m}$. The lower evaporation rates of liquid iron oxide leads to greater survival of iron particles compared with silicates, which enhances their abundance amongst micrometeorites by a factor of 2. The abundance of I-types is shown to be broadly consistent with the abundance and size of metal in ordinary chondrites and the current day flux of ordinary chondrite-derived MMs arriving at Earth. Furthermore, carbonaceous asteroids and cometary dust are suggested to make negligible contributions to the I-type spherule flux. Events involving such objects, therefore, cannot be recognized from I-type spherule abundances in the geological record.

INTRODUCTION

Micrometeorites (MMs) are extraterrestrial dust particles $<2 \text{ mm}$ in size recovered from the surface of the Earth (Genge et al., 2008) and represent that fraction of interplanetary dust population at 1 AU to survive atmospheric entry. Micrometeorites have been collected from Antarctic ice and traps, and deep sea sediments (Brownlee et al., 1985; Maurette et al., 1991; Taylor et al., 2000; Duprat et al., 2007; Rochette et al., 2008) and have provided important information on the population of dust producing small bodies in the solar system including parent bodies not sampled by meteorites. The majority of MMs, however are thought to have affinities to primitive carbonaceous and ordinary

chondrites (Kurat et al., 1994; Genge et al., 1997; Genge et al., 2008; Genge, 2008; Cordier et al., 2011a,b) and include samples of fine-grained matrix, chondrules and refractory inclusions typical of these meteorites.

Iron-nickel metal is a fundamental component of primitive meteorites, in particular in the ordinary chondrites which comprise 3-20 wt% metal (Jarosewich, 1990), and is observed within MMs as small inclusions within unmelted particles and rare immiscible droplets of metal within melted particles (e.g. Genge et al., 2008). Considering that metal grains within chondritic meteorites can have grain-sizes up to several mm, particularly within equilibrated ordinary chondrites (Brearley et al., 1998), the absence of unmelted grains dominated by metal might suggest that the parent bodies of MMs are metal deficient compared with those of meteorites or that metal grains are subject to additional biases in dust production, transport or atmospheric entry.

Iron-dominated particles found to date amongst MMs are I-type cosmic spherules that occur as spheres dominated by wustite and/or magnetite, sometimes containing FeNi metal beads (Taylor et al., 1991; Genge et al., 2008). These particles, like silicate dominated (S-type) cosmic spherules, are formed by extensive melting during atmospheric entry. In Antarctic collections, which are expected to be the least affected by weathering, I-type spherules are present in small abundances of <2% (Taylor et al., 2000; Taylor et al., 2007; Sauvet et al., 2009).

The absence of unequivocal, unmelted metallic MMs and the small abundance of I-type spherules might be a consequence of increased atmospheric entry heating since the higher density of metal grains than silicates will lead to higher peak temperatures (Love and Brownlee, 1994). However, the higher melting temperatures and lower evaporation rates of metal compared to silicates may also result in enhanced survival and compensate for their higher densities. Evaluating the result of entry heating is thus not trivial.

Understanding the entry heating of iron micrometeoroids is of crucial importance in evaluating the Earth's extraterrestrial mass flux since I-type spherules are the most readily collected by magnetic techniques and are the most chemically resistant cosmic dust particles. The preferential recovery of I-type spherules from sediments in the geological record allows the Earth's past extraterrestrial dust flux to be traced (Taylor et al., 1991; Davidson et al., 2007; Heck et al., 2008; Dredge et al., 2010). Extrapolating abundances of I-type spherules in ancient deposits to the overall extraterrestrial dust flux requires knowledge of the relative entry heating survival of these particles (Taylor et al., 2007).

In this paper a numerical model of the entry heating of iron and silicate micrometeoroids is presented, which incorporates a treatment of oxidation, to evaluate the relative proportions of silicate

and metallic micrometeoroids that survive atmospheric entry and to provide constraints on the nature of the sources of I-type spherules.

GENERAL NUMERICAL MODEL

The numerical treatment of atmospheric entry heating used in this paper is based on the model of Love and Brownlee (1991). The equation of motion of a micrometeoroid entering the Earth's atmosphere is described, for a spherical particle, by equation 1. Symbols used in equations in this paper and the values of constants for iron and silicate are summarised in table 1. The negative deceleration term is calculated from the momentum loss of the particle due to collision with a mass of atmospheric gas molecules equivalent to a cylinder of length equal to the speed of the particle and of a diameter equal to that of the particle. This term is a function of atmospheric density, particle density, particle radius and velocity. This formulation of deceleration is based on the assumption that gas flow is within the free molecular flow regime where no development of a bow shock occurs by interaction of backscattered with incident molecules. This is valid, given the mean free path of atmospheric molecules, for particle sizes less than 1 mm (Love and Brownlee, 1991).

$$\frac{\partial v}{\partial t} = g \dot{v} - \frac{3\rho_a v^2}{4r\rho_m} \quad (1)$$

Solution of the equations of motion depend on the calculation of atmospheric density, which varies with altitude, and particle radius, which changes due to evaporation of the particle due to heating. Atmospheric density was calculated by linear interpolation of the 1976 US Standard Atmosphere Model for the stratosphere and requires calculation of altitude of the particle.

Particles with low entry angles (<10°) can pass directly through the atmosphere, performing a grazing incidence encounter, and their altitude thus increases in the final half of their trajectory. Deceleration during such aerobraking manoeuvres often results in a subsequent re-entry if the exit velocity is less than escape velocity. The re-entry velocity of the particle is considered equal to the exit velocity. The cooling of particles outside the atmosphere was calculated assuming heat loss by thermal radiation with no solar insulation using an analytical expression for flight time derived from an elliptical orbit defined by the exit velocity and angle.

The calculation of particle radius with time requires modelling of evaporation rate. The evaluation of mass loss due to evaporation is dependent on whether micrometeoroids are silicate or metallic and are described separately in the following sections. The rate of change of radius can be expressed in terms of mass loss by evaporation by:

$$\frac{\partial r}{\partial t} = \frac{1}{4\pi\rho_m r^2} \frac{\partial m}{\partial t} \quad (2)$$

Surface temperature of the particle may be calculated by consideration of heat flux due to collision of air molecules with the particle, and heat losses by evaporation and thermal radiation. This treatment of energy flux specifically assumes the particle is thermally homogeneous, an assumption shown to be generally true by Love and Brownlee (1991) and only not appropriate where decomposition of volatile-bearing phases acts as an energy sink (Genge, 2006). Energy lost by evaporation can be calculated from the evaporation rate and the latent heat of evaporation L_v . The present model does not consider melting to be a significant heat sink since the latent heat of fusion is two orders of magnitude smaller than that of evaporation. The heat flux of an evaporating micrometeoroid during atmospheric entry can be described by:

$$\frac{\partial q}{\partial t} = \frac{\pi r^2 \rho_a v^3}{2} - L_v \frac{\partial m}{\partial t} - 4\pi r^2 \sigma \epsilon T^4 \quad (3)$$

An expression for surface temperature can then be generated by consideration of the specific heat capacity of the particle since:

$$\frac{\partial q}{\partial T} = mc \quad (4)$$

$$\frac{\partial T}{\partial t} = \frac{\partial q}{\partial t} \cdot \frac{\partial T}{\partial q} \quad (5)$$

These equations give an expression for temperature change in which evaporation is treated by the Langmuir formula.

$$\frac{\partial T}{\partial t} = \frac{1}{rc\rho_m} \left(\frac{3\rho_a v^3}{8} - 3cL_v e^{A-B/T} \sqrt{m_{mol}/T} - \sigma \epsilon T^4 \right) \quad (6)$$

With a system of simultaneous partial differential equations describing the velocity components, altitude, radius and temperature a solution can be approximated by numerical simulation. In this study the Runge-Kutta 4th order method was used to numerically integrate the expressions. A time step was

chosen such that temperature changes by less than 5% in a single timestep. Typical timesteps varied between 0.1 to 0.005 secs and simulations were achieved in 500 to 5000 timesteps. Repeat simulations with different timesteps indicate variation of peak temperature by less than 2%.

Simulation of silicate particles

Silicate particles are modelled to have a constant density of 3000 Kg cm^{-3} and a latent heat of evaporation of $6.050 \times 10^6 \text{ J kg}^{-1}$. Mass loss due to evaporation is modelled using the Langmuir equation and is dependent on the specific heat capacity c , the vapour pressure p_v , the average molecular mass of evaporated species m_{mol} , and the surface temperature as shown in equation 7. The vapour pressure is also temperature dependent and can be described by equation 8 where A and B are constants with values 9.6 and 26,700. Mean molecular mass of evaporated species was assumed to be 45. This treatment of evaporation follows Love and Brownlee (1991) and although not as sophisticated as several more recent treatments that predict evaporation rates from thermodynamic constraints (Vondrak et al., 2008), provides a reasonably accurate agreement with observed relative abundances of melted to unmelted silicate dominated MMs (Love and Brownlee 1993). Simulations of silicate particles within this paper are provided as a comparison to those of iron micrometeoroids.

$$\frac{\partial m}{\partial t} = -4\pi r^2 c p_v \sqrt{m_{mol}/T} \quad (7)$$

$$p_v = e^{A-B/T} \quad (8)$$

Simulation of iron particles

Density and Radius

The simulation of iron micrometeoroids is complex in comparison with silicates due to the oxidation of particles during atmospheric heating. I-type cosmic spherules consist largely of wustite (FeO) and magnetite (Fe₃O₄) but may retain a bead of remnant metal (e.g. Genge et al., 2008). Significant oxidation thus occurs during atmospheric flight. Wustite dominated particles indicate that accretion of mass of up to 23% by reaction with atmospheric oxygen has occurred. The rate of change in mass due to oxidation is crucial to the calculation of the equations of motion and must be specifically considered as an extra term in equation 7.

The rate of oxidation of solid metallic iron has been studied in detail by the metallurgy industry. In the solid state the rate of reaction is controlled by the formation of layers of wustite, with thinner outer layers of magnetite and hematite. The growth in thickness of the oxidised layer can be described by a parabolic rate law due to dependence on diffusion to the oxide-metal interface, where

the parabolic rate constant is temperature dependent and corresponds to the diffusivity of iron through the oxide layer (Young, 2008). The reaction kinetics of iron metal oxidation at 1 atm pressure in air and pure oxygen are well established, however, experiments at lower pressures reveal decreases in reaction rates by several orders of magnitude and divergence from parabolic rate laws (Goursat et al., 1973).

Observations of MMs suggest oxidation reaction rates of iron-nickel metal at sub-solidus temperatures during atmospheric flight are sufficiently low to be negligible. Metal beads within I-type spherules are typically smooth spheres suggesting they have not experienced significant oxidation in the solid state on cooling which, by comparison with the morphology of experimentally oxidised iron, results in re-entrant metal-oxide interfaces (Feng et al., 2005). Iron-nickel metal is also preserved in unmelted coarse-grained MMs and exhibits only evidence for minor oxidation with magnetite and wustite that are typically less than 2 μm in width, even in particles whose glassy mesostases have partially melted, testifying to heating to temperatures of more than the glass transition ($\sim 900^\circ\text{C}$) (Genge et al., 2005). The most significant oxidation of iron-nickel metal within MMs is represented by layered ferrihydrite-dominated alteration products that, due to their low decomposition temperatures, are likely to have formed during terrestrial residence rather than during atmospheric entry (Blackhurst et al., 2004). Oxidation of iron MMs in the solid state will, therefore, be assumed to be unimportant in the current study. Oxidation will be assumed to occur after melting of iron particles.

Iron with molten oxidation products exhibits linear growth of the oxide layer with time at constant temperature (e.g. Young, 2008). Zhang et al (2003) considered oxidation of liquid iron in an oxygen-bearing plasma and assumed that the oxidation will occur when the partial pressure of oxygen in the incident gas reaches a critical value at which the flux of oxygen toward the surface exceeds the flux of metal vapour resulting in the formation of a liquid oxide layer. However, small micrometeoroids ($<1\text{mm}$) are within the free molecular flow regime with negligible interaction occurring between incident and evaporated molecules (Love and Brownlee, 1991). Diffusive transport across an external vapour boundary layer, therefore, need not be considered and only the incident flux due to the particle's velocity and altitude is important. The mass rate of oxidation J can, therefore, be approximately given by:

$$J = \gamma \rho_o \pi r^2 v \quad (9)$$

where the atmospheric density of oxygen ρ_o is calculated by linear interpolation of the 1976 US standard atmosphere and only total oxygen is considered with no distinction between monatomic and molecular oxygen. This is reasonable since the incident kinetic energy exceeds that required for bond

breaking in molecular oxygen. The factor γ is a constant related to the efficiency of the surface transfer of oxygen and will be considered as unity in these simulations. The validity of this assumption is considered in the discussion of this paper.

The expression for oxidation in the liquid state allows the increase in mass of particles to be considered together with mass loss by evaporation.

$$\frac{\partial m}{\partial t} = -\frac{\partial m_{evap}}{\partial t} + \gamma \rho_o \pi r^2 v \quad (10)$$

The volume fraction of oxide to metallic iron liquid is also important due to the density contrast between these liquids. Increases in the relative mass of oxide to metallic liquid will result in an increase in radius of the particle. Wustite liquids have a density of 4400 kg m^{-3} (Millot et al, 2009) whilst metallic iron liquids have densities of 7000 kg m^{-3} at 1800K (Drotning, 1981). Thermal expansivity of both metallic and oxide iron liquids are $<5\%$ over the liquid field and will be ignored. The equilibrium phase relations of the Fe-O system (Fig. 2; Darken, 1946) indicate negligible miscibility between metallic and oxide iron liquids at temperatures $<2300\text{K}$ and a decreasing two phase field with complete miscibility at temperatures above 2900K . In this paper we will assume that two immiscible liquids are present and represent pure metallic iron and an iron oxide liquid with a wustite composition.

The rate of change of density of the particle will depend on the rate of growth of the iron oxide liquid by oxidation of metallic iron liquid coupled with mass loss by surface evaporation. The rate of density change can, therefore, be evaluated by separate calculation of the change in mass of the oxide and metal liquids.

$$\frac{\partial m_m}{\partial t} = -\gamma \frac{M_{Fe}}{M_O} \rho_o \pi r^2 v \quad (11)$$

$$\frac{\partial m_{ox}}{\partial t} = -\frac{\partial m_{evap}}{\partial t} + \gamma \frac{M_{FeO}}{M_O} \rho_o \pi r^2 v \quad (12)$$

Note that since the particle density, and thus partly the radius, is dependent on the mass fraction of oxide to metal, particle density was only calculated until the iron liquid is completely consumed, after which the density of wustite liquid is used. A further complication in the mass loss and density change of iron micrometeoroids may result from the separation of metallic droplets under the high decelerations experienced by particles. This is a complex process involving separation of two

liquid droplets and requires consideration of their surface tensions and deformation of liquid drops during flight. The timescales required for separation are crucial but not easily calculated. Observations of I-type spherules indicate that a proportion retain their FeNi metal beads, whilst others may have lost them during flight. In this paper we will assume metal droplets are retained, however, this caveat will be discussed later and a correction applied to final masses to estimate the effect of metal separation on the size distribution.

Evaporative mass loss

The mass loss by evaporation requires careful consideration in the context of an iron micrometeoroid that is being oxidised by atmospheric oxygen. Observations of I-type spherules suggest that iron-oxides either dominate spherules or occur as a shell surrounding an off-centre droplet of FeNi metal (Fig.1). These observations are consistent with the phase relations of the system Fe-O in which a two liquid field exists between wustite and pure iron metal compositions. The addition of oxygen to a metallic iron liquid, therefore, results in immiscible iron oxide and a metallic iron liquid. The observation that iron-oxides form an external shell in particles with metal beads, and the absence of iron oxide liquids within metal beads, strongly implies that iron oxide liquids wet the surface of molten iron micrometeoroids. Mass loss, therefore, will occur principally by evaporation of the iron oxide liquid at the surface rather than the metallic liquid. This is an important distinction since the evaporation rate of iron oxide liquids is an order of magnitude less than metallic iron liquids.

The nature of the iron oxide liquid is an important consideration influencing the oxidation rate. I-type spherules often contain an assemblage of wustite (FeO) and magnetite (Fe₃O₄) within their oxide portions, even in those that contain metal beads (Genge et al., 2008; Parashar et al., 2010). The presence of iron-nickel metal, wustite and magnetite is a strongly non-equilibrium assemblage. Phase relations, however, indicate that on cooling the wustite partly decomposes to magnetite. The addition of oxygen at low temperatures, after the crystallisation or loss of the metal bead, could also enhance the magnetite content. This scenario is suggested here to be realistic since during the final stages of crystallisation particles have penetrated to the lower altitudes where partial pressure of oxygen is the highest. Since magnetite can be expected to form as a result of the final stages of oxidation during entry heating, an oxide liquid with a wustite stoichiometry, consistent with metal-oxide immiscibility, is used to calculate the relative volume of metal and oxide liquids.

The calculation of evaporation rates based on iron oxide liquids differs from that of Yada et al. (1996) who argued that the metal bead is always exposed at the leading edge of the spherule. However, observations of I-type spherules do not support exposed metal cores and suggest that cores are off-centre but covered by a film of iron oxide liquid. As long as the oxide liquid can be considered

well mixed, oxygen diffusion across the oxide melt layer does not need to be considered in the oxidation rate. Furthermore, although metal beads are likely to migrate to the leading edge of spherules, the curvature of the metal bead compared to the oxide spherule will ensure that mass loss is dominated by evaporation from the oxide liquid. In this simulation the evaporation rate of FeO liquids experimentally measured by Wang et al. (1994) is used to calculate mass loss and provides a vapour pressure of:

$$\log(p_v) = 11.3 - 2.0126 \times 10^4/T(K) \quad (13)$$

A complication occurs when evaporation rate exceeds oxidation rate since the oxide liquid could completely evaporate to expose the iron liquid. In practice, however, complete removal of the oxide liquid by evaporation was not observed in any simulation. A related problem occurs when the metallic liquid is completely consumed. At this point further mass and heat gain through oxidation was not considered.

Heat of oxidation

An important consideration in the calculation of the temperature of iron particles oxidizing during atmospheric entry is the heat of oxidation. Oxidation is strongly exothermic with a heat of formation of 3716 kJ/Kg of oxide, which is of a similar magnitude to that lost to evaporation and thus must be evaluated in the heat flux expression.

$$\frac{\partial q_{ox}}{\partial x} = \Delta H_{ox} \frac{\delta m_{ox}}{\delta t} \quad (14)$$

RESULTS

Comparison between silicate, iron metal, iron oxide, and oxidizing iron meteoroids

Simulation of the atmospheric entry of micrometeoroids composed of silicates, iron metal, iron oxide and mixtures of iron metal and iron oxide were performed for particles with an initial radius of 50 μm at an entry angle of 45° and a entry velocity of 12.0 km s^{-1} in order to allow comparison between their thermal and dynamic behaviour during entry heating. The iron metal only micrometeoroid was considered not to undergo oxidation to allow comparison to the oxidation model. The temperatures and radius of particles predicted are shown in figure 3.

Simulation of the silicate micrometeoroid predicts a peak temperature of 1690.6 K attained at an altitude of 85.86 km and a final particle radius after evaporation of 37.5 μm consistent with the

results of Love and Brownlee (1991). Assuming a solidus temperature of 1573K this particle would have experienced partial melting during atmospheric entry.

The results for the iron micrometeoroid indicate the particle would experience a higher peak temperature of 2225.8 K at an altitude of 80.31 km. The higher temperature attained by this particle is largely due to its penetration to lower altitude due to its higher density, however, the low vaporization rates of iron metal, and thus lower heat loss through evaporation are also a factor. The final radius of the particle at 47.9 μm due to the lower evaporation rate of metal compared with silicates. Assuming a melting temperature of 1809K (for pure Fe) this particle would have melted to form a spherule.

Simulation of an iron oxide only micrometeoroid illustrates the strong dependence on density of peak temperature at constant entry velocity and angle, with a peak temperature of 2020.8 K attained at 83.0 km altitude. The lower vaporisation rate of iron oxides than iron metal results in less mass loss during heating resulting in a final radius of 49.6 μm .

In the simulation of the mixed metal-oxide micrometeoroid, in which oxidation is considered, the particle initially consists entirely of iron metal but on melting oxidises at its outer surface resulting in a gradual decrease in net density and an increase in mass with additional heat generated by oxidation. The peak temperature predicted for this simulation is 2215.0 K attained at 80.7 km and unsurprisingly is intermediate between that of the iron only and iron oxide only particles, but is closer to the peak temperature of the iron only micrometeoroid due to the dependence of oxidation rate on altitude. The temperature-time profile also indicates a more rapid cooling rate than any of the other simulations. The cooling rate during atmospheric entry is considerably lower than the black body radiative cooling rate of particles of this size due to the continued heating by collisions with air molecules. Cooling rate of micrometeoroids are thus crucially dependent on their dynamic behaviour. The rapid cooling rate of this particle arises since its heating rate is decreasing rapidly with time as its density decreases, whilst there is only a small change in cross-sectional area.

The final radius predicted by the model for this oxidizing iron particle is 52.0 μm , larger than the initial particle that entered the atmosphere. This increase in radius is due to the decrease in density as iron liquid is consumed by oxidation to form lower density iron oxide liquid, and the increase in mass due to the reaction of atmospheric oxygen. The predicted mass proportion of remnant metal present in the particle is 0.23. The change in radius of the particle with time is complex due to the competing processes that influence particle radius.

The Thermal Behaviour of Silicate and Iron Micrometeoroids

The peak temperatures calculated for silicate and iron micrometeoroids are shown in figure 4, and consistent with expectation, show increases in temperature with particle size, entry velocity

and entry angle. Iron micrometeoroids attain significantly higher peak temperatures than silicate particles by 300-800K owing to their higher densities, which result in penetration to lower altitudes where atmospheric pressures are higher, causing more significant heating.

The melting temperatures of silicates (1573K, solidus temperature) and iron (1809K) are also shown in figure 4 and indicate that the size threshold for unmelted silicate particles is larger than for unmelted iron meteoroids at all entry angles and velocities. At an entry angle of 45° and entry velocity of 12 km s⁻¹, for example, a silicate particle up to ~40 μm in radius can survive atmospheric entry without melting whilst an iron particle must be less than ~20 μm in radius to escape melting.

The duration of heating for particles is shown in figure 5 as the time spent at temperatures above their solidi and is a maximum of 12 seconds for the entry parameters considered. The duration of the heating pulse increases with decreasing entry angle by a factor of 3-4 from entry angles of 90° to 15° degrees. There is a slight dependence on particle size with larger particles remaining molten for slightly longer periods than smaller particles in particular for low angle particles. The higher density of iron micrometeoroids also leads to slightly longer periods above the solidus than silicate particles of similar size, entry velocity and entry angle.

The altitude at which micrometeoroids attain peak temperature is also an important consideration in the model of iron particles since, together with velocity, it determines the oxidation rate experienced. The peak temperature altitude for iron micrometeoroids are shown in figure 6 and vary between 100 and 65 km. Altitude decreases with increasing particle size, entry angle and particle radius, however, high velocity, large particles experience peak temperature at higher altitude than low velocity particles due to their rapid mass loss by evaporation.

Final Particle Radii

The final particle radii of silicate and iron micrometeoroids are shown in figure 7 and reflect mass loss by evaporation and, in the case of iron particles, mass and density change by oxidation. Final relative particle radii decreases with increasing initial particle size, increasing entry angle and in particular with entry velocity. Silicate particles exhibit extreme mass loss and decrease in particle radii at higher velocities. At 18 km s⁻¹ most particles initially larger than 100-200 μm have lost sufficient mass to produce residue spherules less than 20 μm in radii, a similar radius to low velocity particles with an initial radii of 30 μm. At higher velocities the majority of larger silicate particles entirely evaporate.

Mass losses calculated for iron micrometeoroids are significantly less than those of silicate particles principally due to the significantly lower evaporation rate of iron oxide liquids. Iron spherules exhibit relative final radii 1.5 to 3.0 times the size of silicate micrometeoroids with the same initial radii. Most iron oxide droplets completely evaporate at entry velocities of >22 km s⁻¹. Despite their

lower mass loss in comparison with silicates, iron micrometeoroids experience significant decreases in mass. Particles 200 μm in radius with an entry velocity of 12 km s^{-1} and angle of 45 degrees, for example, has a relative final radius of 0.72 and has experienced a mass loss of 63%. This value is within the range of 55-77% mass loss estimated from oxygen isotope systematics of similar sized spherules by Engrand et al., (2005) and 36-96% by Xue et al., (1996) from nickel isotopes.

Iron micrometeoroids with initial radii $<150 \mu\text{m}$ exhibit a net increase in their radii over the duration of heating due to the growth of iron oxide mantles, owing to the lower density of iron oxide, and mass gain of oxygen from the atmosphere. Iron micrometeoroids with low entry angles are predicted to experience larger net increases during entry heating.

Radii of oxidizing iron micrometeoroids

Given the complex nature of radii change predicted for oxidizing iron micrometeoroids a series of simulations were performed to investigate how entry parameters and particle size influence the change in radius. Typical radius vs time profiles are shown in figure 8.

The radius-time profiles for show some broadly similar features. Most profiles exhibit an initial small radius increase immediately after melting due to initial oxidation and the formation of iron oxide melt. In particles with high peak temperature (i.e. high entry velocity and angle), however, this initial radius increase is negligible. Decreases in radii due to evaporation occur for most particles over the high temperature portion of deceleration with a magnitude depending on peak temperature, however, particles with the lowest peak temperatures, with low entry velocities and/or entry angles have minimal or no decrease in particle radii. Most micrometeoroids also exhibit an increase in radii during cooling from peak temperature prior to solidification due to oxidation with only those particles which attain the highest peak temperatures lacking a significant post-heating increase due to rapid mass loss and deceleration.

The Abundance of Metal Beads

The relative mass proportion of metal beads to iron oxide mantles are shown in figure 9. The presented model utilises a maximum estimate of the oxidation rate by assuming that all incident oxygen atoms react to form iron oxide liquid as long as the particle is above its solidus temperature. The mass proportion of metal thus is a lower limit.

The results indicate a wide variation in the survival of metallic iron beads with entry velocity, entry angle and particle size. For low velocity iron MMs ($<16 \text{ km s}^{-1}$) metal survival is restricted to particles with small initial radii ($<100 \mu\text{m}$) and increases with decreasing entry angle ($<150 \mu\text{m}$).

Metal survival is more complex within higher entry velocity particles. Like low velocity particles metal survival increases with decreasing size for particles below $\sim 50 \mu\text{m}$ in radius, however, a region of metal survival appears at larger sizes ($>100 \mu\text{m}$ radius) and steeper entry angle ($>40^\circ$) in

which comprises up to 40% mass of the particle. With increasing entry velocity this region of metal survival expands to higher particle radii and lower entry angle with particles comprising up to ~50% mass of metallic iron. A band of low metal survival, however, still exists at lower entry angles with virtually no metal retained by particles. The survival of metal at higher velocities is the result of significant mass loss by evaporation which results in loss of oxide liquid and rapid cooling minimising the opportunity for further oxidation.

DISCUSSION

Oxidation and entry heating

The results of the simulations suggests that oxidation has a significant effect on entry heating of iron micrometeoroids, however, the model used to calculate oxidation rate in these calculations represents a maximum estimate since it is dependent on the incident flux of oxygen at the surface of the particle, albeit with loss of oxide due to evaporation. The model predicts the survival of metal in many particles with typical mass proportions of <0.3. The abundance of metal in I-type spherules is, however, somewhat uncertain due to the low numbers of these particles recovered outside of deep sea sediments, and owing to sectioning effects that will under-estimate the metal abundance. In deep sea sediments abundances of metal beads of >30% have been observed (Taylor et al., 2007; Parashar et al., 2010), however, considering the use of magnetic separation techniques this may be an overestimate. Amongst Antarctic particles reported by Genge et al., (1997) no metal beads were observed amongst 13 I-type spherules, whilst ~50% of 65 I-types contained metal in the South Pole Water Well (Taylor, pers. communication) and ~30% amongst 45 I-types from Larkman Nunatak moraine (Genge, unpublished data) . Observations of Antarctic I-type spherules, therefore, suggest less than half retain metal beads, but do not provide definitive size distributions for comparison to the models.

The numerical results presented here suggest that metal survives oxidation only within particles with radii <150 μm at low entry velocities with the largest abundance of metal in the smallest particles. The model suggests, however, that metal beads can survive in larger particles with high entry velocities and low entry angles due to increased evaporation of the iron oxide mantle which allows more rapid deceleration and minimises opportunity for oxidation. These particles, however, produce significantly smaller residual spherules.

Brownlee et al., (1984) noted that in deep sea I-type spherules metal beads are not observed in particles larger than 150 μm in radius, although, some larger particles (<200 μm) have since been identified (Engrand et al., 2005). Platinum-group element nuggets, suggested to form by complete oxidation of metal and fractional evaporation, are also observed in large magnetite-rich spherules (Brownlee et al., 1984; Rudraswami et al., 2011). The numerical results, therefore, are consistent with

observations of I-types since they indicate complete oxidation of metal in larger particles and furthermore imply that the majority of particles have low entry velocities with only rare examples of large particles retaining metal originating from higher velocity dust.

The rarity of large I-type spherules with metal beads and the significant abundance of platinum group nuggets (Brownlee et al., 1984; Rudraswami et al., 2011) suggests that oxidation is an efficient process. Simulations of particles with initial radii of 200 μm , 45° entry angles and velocities of 12, 16 and 20 km s^{-1} were conducted to test the relict metal abundances present at different values of the oxidation efficiency coefficient. At values of 0.9 the relict metal abundance within the 16 and 20 km s^{-1} reaches a mass proportion of 0.9 significantly larger than observed in I-type spherules. These results imply a value to 1.0 for the efficiency constant is realistic, albeit with the requirement that significant separation of iron oxide and iron metal liquids does not occur.

The simulation results indicate that metal abundance within I-types is dependent on both oxidation and on evaporation of the iron oxide liquid mantle. In no simulation, however, did the mass loss by evaporation completely remove the oxide liquid and allow direct evaporation of metal. This result is contrary to estimates of evaporative loss from I-types on the basis of oxygen and iron isotope compositions by Engrand et al., (2005) who calculated fractional mass losses of 55-77% from oxygen and 69-85% from iron isotopes implying a loss of 40% mass of iron prior to oxidation. Pre-oxidation evaporation of metal, however, would be difficult to achieve without a lower efficiency for oxidation, which as discussed above, leads to metal bead survival in large spherules that are contrary to observation. Loss of iron oxide mantles allowing evaporation of metal are also not consistent with the lower evaporation rate of iron oxide liquid than metallic liquid. A possible explanation could be additional mass fractionation of iron isotopes by exchange between immiscible metal and oxide liquids followed by separation of a small residual metal bead.

Separation of immiscible liquids

Separation of metallic iron liquid beads from iron oxide during atmospheric flight is likely to occur due to the large decelerations experienced by particles. The separation of metal liquid droplets from the accumulated oxide liquid would be expected to change the deceleration and heating profiles of particles since splitting would generate two particles, a high density metal liquid particle and a lower density liquid oxide particle. The significant decrease in particle radii and change in particle densities would alter the dynamic behaviour during atmospheric flight.

The low-Ni contents of many I-type spherules testify to the separation of metal beads during flight since Ni is preferentially retained by the metal bead during oxidation (Brownlee et al., 1983; Taylor et al., 1991; Genge et al., 1998). Morphological evidence for removal of metal beads also occurs

in the form of exterior protrusions on the surface of particles suggesting separation immediately prior to solidification.

Two factors will be important in whether metallic iron droplets separate from iron oxide liquids, the relative volume of metal to iron oxide liquid, and the contact angle at the interface between the liquids. If the contact angle of an iron oxide liquid on the surface of a metallic iron liquid is large it will form a droplet on the surface, otherwise it will wet the surface forming a meniscus that will resist separation. Whether a liquid will wet a surface can be determined by the spreading factor S (e.g. Rosen, 2004):

$$S = \lambda_{metal} - (\lambda_{oxide} + \lambda_{oxide-metal}) \quad (15)$$

where λ is the surface tension of the liquids and the interfacial tension between the liquids. Positive values of the spreading parameter indicate a liquid wets the surface, whilst negative values indicate the liquid will form droplets with a large contact angle and potentially be able to separate. The surface tension of iron oxide liquids is $\sim 0.6 \text{ N m}^{-1}$ (Millot et al., 2009) and the surface tension of metallic iron liquids is $\sim 1.9 \text{ N m}^{-1}$ (Brillo et al., 2005). The interfacial tension between oxide and metal liquids is unknown, however, given the broadly similar metallic structure of the liquids, we can expect the interfacial tension to be lower than the surface tension of either liquid to vacuum giving positive values of the spreading factor. Consequently iron oxide liquids will wet the surface of metal beads. Separation of metal droplets from iron oxide will require the flow of iron oxide liquid out of the film wetting the surface which would be most efficient where metal droplets are small in comparison to the iron oxide requiring flow over a smaller distance.

Figure 1d shows an I-type spherule recovered from the South Pole Water Well (courtesy of Susan Taylor) that illustrates the behaviour of oxide liquids during separation. Although the metal bead in this spherule is close to separation, a thin film of oxide liquid remains because of its low contact angle with the metal liquid, although withdraw of the liquid appears to have been occurring prior to solidification. If it is assumed this particle is representative, and that metal separation was about to occur, a radius ratio of < 0.4 could be taken as a threshold for bead separation. This gives a decrease in radius of only 0.98 for this particle. Such small decreases in radius, in particular later in deceleration when metal bead size is minimised, will have only a small effect on the dynamical behaviour of particles. The conclusion that metal separation has a relatively minor effect is also consistent with the observation of platinum group element nuggets which require minimal separation of the metal in which these elements become concentrated during oxidation (Brownlee et al., 1984; Rudraswami et al., 2011).

Cavities and surface protrusions

Spherical to elliptical cavities, and unusual surface protrusions, are observed on I-type spherules and have been suggested to be due to the separation of metallic liquids during deceleration. Feng et al. (2005) suggest that crystallisation of I-type spherules from their surface could explain the formation of spherical cavities due to contraction. Support for this observation is provided by rare examples of I-types that show radiating crystal structures with an internal void (e.g. Genge et al., 1997), however, the smooth surfaces of voids, in comparison to geodes that form by inwards crystallisation, suggest cavities existed prior to crystallisation, although some irregular voids in I-types probably do form by this mechanism (e.g. Fig 1b).

An alternative explanation for cavities and protrusions in I-type spherules is suggested by the results of oxidation experiments of metallic liquids performed by Wang et al. (1994) who observed vesicle formation under conditions of ambient heating in an oxygen-rich atmosphere. These observations suggest that vesicles may form from gaseous oxygen exsolved on cooling of iron oxide liquids, although SO₂ gases formed by volatilisation of a sulphide component are also possible. Gas loss during vesicle separation is suggested here as a possible explanation for the formation of surface deposits of iron oxide (Fig. 1e,f) and are thus not necessarily due to the separation of metal beads.

The abundance of unmelted iron micrometeorites

Unmelted iron MMs have yet to be unequivocally identified, however, Maurette et al. (1987) reported unmelted metal grains from Greenland cryoconite. In part this may reflect the susceptibility of metallic iron to terrestrial weathering, however, iron-nickel metal does survive close to the surface of many unmelted MMs, albeit sometimes with development of weathering rinds composed largely of ferrihydrite (Blackhurst et al., 2004). The absence of ferrihydrite dominated particles with relict metal, however, does imply that unmelted iron MMs are present in only very small abundances amongst particles collected from Antarctica (<0.01%).

The results of the simulations presented here explain the very low abundance of unmelted iron particles amongst particles with diameters >50 µm, since even at the lowest entry velocities iron micrometeoroids melt during deceleration except at entry angles <30°. This implies that unmelted iron MMs are most likely to be present at sizes <50 µm.

The abundance of I-type spherules

The abundance of I-type spherules in Antarctic micrometeorite collections are very small at <2% whilst in deep sea collections the abundance is significantly larger at >30% (Taylor et al., 2007). Iron oxides are, however, highly resistant to chemical weathering compared with silicates and the large abundance of I-types within deep sea sediments is undoubtedly due to both preservation factors

and the use of magnetic separation in their collection. I-type spherules are, therefore, a very minor proportion of MMs but are very important to understand since they are the most likely to be preserved amongst particles recovered from ancient deposits in the geological record (Taylor et al., 1991; Davidson et al., 2007; Heck et al., 2008; Dredge et al., 2010). Understanding how the surviving I-type population relates to the pre-atmospheric population of precursors is thus highly important in correlating between collections, as discussed by Taylor et al., (2000), and evaluating the causes of changes in the extraterrestrial dust flux.

The simulations of oxidizing iron micrometeoroids conducted in this work suggest that they are more likely to survive atmospheric entry without complete evaporation than silicate particles with significant survival of particles at entry velocities $<16 \text{ km s}^{-1}$. The low abundances of I-type spherules, therefore, cannot be explained by evaporative mass loss, which should enhance their abundance relative to silicate particles and imply either low metal to silicate abundances within the interplanetary dust population, or biases due to dust production or transport. The implications for the nature of the parent bodies of MMs will be discussed below.

IMPLICATIONS

The parent bodies of I-type spherules

The numerical results presented in this paper indicate that iron micrometeoroids lose less mass during atmospheric entry than silicate particles due to their low evaporation rates and are more likely to survive atmospheric entry. In the absence of other biases the abundance of iron particles amongst MMs would, therefore, be expected to be enhanced by around a factor of 2 compared with the metal abundance amongst the pre-atmospheric dust population and thus the metallic iron abundance on their parent bodies. I-type spherules, however, have a very small abundances compared to S-type (silicate) spherules that would suggest average parent body abundances of <1 volume% in the absence of other biases.

Metal abundance, however, is not the only factor that needs to be evaluated in assessing the source of I-type spherule precursors. The size distribution of metal grains within potential parent bodies is also crucially important since I-type spherules clearly formed by oxidation of individual metal grains with no significant silicate content. The size of metal on the parent body, when liberated, must be sufficient to generate the observed spherules and required physical segregation from silicates during dust production. Although the size distribution of I-types is poorly constrained examples up to $\sim 500 \mu\text{m}$ have been reported (Brownlee et al., 1984; Rudraswami et al., 2011) which with mass loss of $>90\%$ experienced during entry heating would imply precursor grains $>650 \mu\text{m}$.

The parent bodies of the majority of MMs are thought to have affinities to the carbonaceous and ordinary chondrites (Kurat et al., 1994; Genge et al., 1997; Genge et al., 2008; Genge, 2008;

Cordier et al., 2011a,b), meteorites that are most likely to be samples of asteroids, although samples of comets are likely amongst the carbonaceous fraction (Noguchi et al., 2015; Nesvorný et al., 2010; Duprat et al., 2007). The majority of fine-grained MMs are dominated by clay minerals, or their thermal decomposition products, and closely resemble those of CI, CM2, and CR2 chondrites whose parent asteroids have experienced extensive aqueous alteration (Genge et al., 1997). Metal is absent from CI chondrites and within CM2 chondrites only occurs as small grains (<100 µm), largely within relict chondrules (Kimura et al., 2011; Brearley et al., 1998), of insufficient size to be the precursors of I-type spherules. Within CR2 chondrites metal is relatively common but is still largely restricted to the chondrules and their rims (Brearley et al., 1998) but may be of sufficient size to generate spherules <100 µm in size if liberated from silicates during collisional dust production. The abundance of metal within CM2 chondrites is <0.14 wt% (Jarosewich, 1990) whilst CR2 chondrites have abundances of 3.7-7.4 vol% (Weisberg et al., 1993). Carbonaceous chondrite-like parent bodies, whether asteroidal or cometary, that had been strongly altered by water, are thus unlikely to be significant sources of I-type spherules.

The nature of cometary parent bodies is highly uncertain, however, observations of anhydrous IDPs (Reitmeijer, 1998), STARDUST samples (Zolensky et al., 2006) and enstatite whisker-bearing MMs (Noguchi et al., 2015) indicate that they are likely to lack metal grains larger than a few tens of µm in size and are, thus, unlikely to parent bodies for I-type spherules. This suggests that I-type spherules recovered from ancient sediments reflect only asteroidal dust production and cannot be used to identify the influx of comets into the inner solar system.

Ordinary chondrite-like parent bodies are thought to contribute to MMs. Around 70% of unmelted coarse-grained MMs have been shown to have strong affinities to equilibrated and unequilibrated ordinary chondrites, representing approximately 25% of all particles (Genge, 2008). Cordier et al. (2011a,b) have also demonstrated on the basis of olivine Ni contents, and oxygen isotope compositions that up to 50% of silicate dominated cosmic spherules (S-types) are derived from ordinary chondrites, rather than carbonaceous chondrites.

Ordinary chondrites are primitive meteorites that contain relatively abundant iron-nickel metal. LL chondrites (low iron, low metal) contain the least abundances of metal at 1.1-1.9 (average 1.6) vol%, whilst H chondrites contain ~1.5-7.5 (average 6.8) vol%, with the L group having intermediate values (estimated from compositions in Jarosewich, 1991). Studies of ordinary chondrite-like unmelted MMs have shown that at least L and H chondrite materials are present amongst MMs (Genge, 2008). The size distribution of metal has been studied within a limited number of ordinary chondrites by X-ray tomography and suggests 80% of metal grains are <750 µm in size, with a small proportion of grains up to several millimetres in size (Friedrich et al., 2008). Size

distributions from enstatite chondrites also suggest that metal coarsening during parent body metamorphism occurs (Schneider et al., 2008). Ordinary chondrites, in particular equilibrated ordinary chondrites, therefore, are likely to have metal in sufficient abundance and at sufficient size to generate I-type spherules.

The abundance of I-types that would be expected if the pre-atmospheric population consists of 50% metal free carbonaceous chondrite-like and/or cometary particles and 50% ordinary chondrite-like materials, similar to suggested by Cordier et al. (2011a,b), consisting of an equal proportion of L, LL, and H chondrite materials, is approximately 2 vol%, similar to the observed value of I-types. The results of the simulations, however, suggest that I-type abundances will be enhanced by approximately a factor of 2, consistent with an abundance of metal-bearing ordinary chondrite particles of ~20% similar to the abundance of these materials suggested by coarse-grained unmelted MMs (Genge, 2008). Given that total metal contents of the chondrites do not reflect the abundance of grains large enough to produce I-types, however, the abundance of ordinary chondrite materials is likely to be closer to that suggested by Cordier et al. (2011a,b).

The presence of FeNi metal grains derived from the parent asteroids of iron meteorites must also be considered. Iron meteorites comprise ~5% of the meteorite flux, however, their abundances are strongly enhanced amongst recovered meteorites due to their preferential survival of atmospheric entry, suggesting a much lower pre-atmospheric abundances. Furthermore, the observation that basaltic MMs make a very small contribution to the MM flux (Cordier et al., 2011c), despite the significant flux of HEDs, demonstrates that the meteorite flux is a poor guide to the abundance of MM types. Given that the ordinary chondrite flux can provide sufficient numbers of I-type spherules there seems little requirement for a significant contribution of differentiated metal amongst the Earth's current day extraterrestrial dust flux.

The generation of I-type particles from S-type cosmic spherules by the separation of metal droplets also needs consideration (e.g. Genge et al., 1998; Taylor et al., 2000). Most metal beads within S-type spherules, however, are relatively small (<50 μm) and cannot, therefore, be the source of the majority of I-types. The possibility of separation of metallic droplets from meteorites during their atmospheric entry can also be discounted as a major source of I-type spherules on the basis of the much smaller flux of meteorites than micrometeorites (Love and Brownlee, 1993).

Evaluating the sources of I-type cosmic spherules on the basis of their compositions are complicated by the effects of partial evaporation, oxidation and, in some cases, loss of residual metal beads. The mass Fe/Ni ratios of I-types range from 2330 to 10 whilst Cr/Ni ranges from 16×10^{-3} to 17.3×10^{-3} (Herzog et al., 1999; Engrand et al., 2005). Herzog et al (1999) considered the compositions of deep sea I-type spherules in detail, including estimates of pre-evaporation abundances based on

measured Fe, Ni and Cr isotope compositions, and concluded they most closely resemble metal from chondritic meteorites. The Cr/Fe abundances in I-types were suggested to be most compatible with metal from carbonaceous chondrites, since ordinary chondrites have lower abundances in the metal phase. Ordinary chondrites, in particular equilibrated meteorites, however, contain abundant chromite (Brearley et al., 1998). The presence of inclusions this phase within the metallic precursors of I-type spherules could make their compositions compatible with ordinary as well as carbonaceous chondrites.

The constraints of the size and abundance of metal within chondrites would suggest that ordinary chondrite-like parent bodies are the most likely source of metal dust grains that generate I-type spherules. This conclusion also agrees with the observation that low entry velocities, most consistent with an asteroidal source, are required to ensure survival of metal beads. Further constraints on the identity of the parent bodies of I-type spherules may, however, be difficult to provide due to the complex evolution of their elemental and isotopic compositions by fractional evaporation and partitioning between metallic and oxide liquids. Additional complexity may also arise due to the association of iron sulphides and chromite with metal in chondrites (e.g. Brearley et al., 1998). The simulation results presented in this paper do not apply to sulphide-metal mixtures which will have lower overall density than metal only particles, however, rapid degassing of sulphides might be expected to generate smaller residual I-type particles.

CONCLUSIONS

Simulation of the atmospheric entry of iron micrometeoroids suggest that their behaviour is complex due to the competing effects of mass gain and density change by oxidation and evaporation of the external mantle of oxide liquid. Simulations show that low velocity (12 km s^{-1}) and low entry angle particles ($<30^\circ$) can gain net mass from the atmosphere producing unique dynamic behaviour. Metal bead survival is predicted to occur within small, low velocity particles and to be enhanced by low entry angles, but also occurs for large high velocity particles that experience significant evaporative mass loss of the liquid oxide mantle, consistent with observations of I-type spherules. The peak temperatures predicted for iron micrometeoroids are significantly higher than those of silicates, however, the lower evaporation rates of oxide liquids ensure that they are more likely to survive atmospheric entry than silicate particles of equivalent size. The abundance and size of I-type spherules observed in Antarctic collections is broadly consistent with the nature ordinary chondrite parent bodies and the flux of ordinary chondrite MMs suggesting these are the predominant parent bodies of these objects. Carbonaceous chondrite asteroids and cometary sources should make little or no contribution to the flux of I-type spherules and events involving such objects will not be observable from I-type spherules recovered from the geological column.

Acknowledgements

Susan Taylor is thanked for providing images of I-type spherules containing iron nickel metal beads. Susan Taylor and Carole Cordier are thanked for providing helpful and insightful reviews. Carole Cordier in particular is thanked for highlighting the role of sulphides. This study was funded by the Science and Technology Council (STFC), grant number ST/J001260/1.

REFERENCES

Blackhurst R. L., Genge M. J. and Grady M. M. 2004. Microbial D/H fractional in extraterrestrial materials: Application to micrometeorites and Mars. 35th Lunar and Planetary Science Conference, March 15-19, 2004, League City, Texas, abstract no.1584.

Brillo J. and Egry I. 2005. Surface tension of nickel, copper, iron and their binary alloys. *Journal of Materials Science* 40:2213-2216.

Brearley A. J. and Jones R. H. 1998. Chondritic meteorites. In *Planetary Materials*, Vol. 36, edited by J. J. Papike, Mineralogical Society of America. pp 1-191.

Brownlee D. E. and Bates B. 1983. Meteor ablation spherules as chondrule analogs. In *Chondrules and their Origins*, edited by E. A. King, Lunar and Planetary Institute. pp 10-25.

Brownlee D. E., Bates B. A. and Wheelock M. M. 1984. Extraterrestrial platinum group nuggets in deep-sea sediments. *Nature* 309:693-695.

Cepelcha Z., Borovicka J., Elford W. G., Revelle D. O., Hawkes R. L., Porubcan, V., Simek M. 1998. Meteor phenomena and bodies. *Space Science Reviews* 84:327-471.

Cordier C., Van Ginneken M. and Folco L. 2011a. Nickel abundance in stony cosmic spherules: constraining precursor material and formation mechanisms. *Meteoritics and Planetary Science* 46:1110-1132.

Cordier C., Folco L. Sauvet C., Sonzogni C. and Rochette P. 2011b. Major, trace element and oxygen isotope study of glass cosmic spherules of chondritic composition: The record of their source material and atmospheric heating. *Geochimica et Cosmochimica Acta* 75: 5203-5218.

Cordier C., Folco L. and Taylor S. 2011c. Vestoid cosmic spherules from the South Pole Water Well and Transantarctic Mountains (Antarctica): A major and trace element study. *Geochimica Cosmochimica Acta* 75:1199-1215.

Davidson J., Genge M. J., Mills A. A., Johnson D. J., and Grady M. M. 2007. Ancient cosmic dust from Triassic salt. 38th Lunar and Planetary Science Conference, Lunar and Planetary Science XXXVIII, held March 12-16, 2007 in League City, Texas. LPI Contribution No. 1338, p.1545.

Darken L. S. 1946. The system iron-oxygen. II. Equilibrium and thermodynamics of liquid oxide and other phases. *Journal of the American Chemical Society* 68:798-816.

Dredge I., Parnell J., Lindgren P., and Bowden S. 2010. Elevated flux of cosmic spherules (micrometeorites) in Ordovician rocks of the Durness Group, NW Scotland. *Scottish Journal of Geology* 46:7-16.

Drotning W. D. 1981. Thermal expansion of iron, cobalt, nickel and copper at temperatures to 600K above melting. *High Temperatures and High Pressures* 13: 441-458.

Duprat J., Engrand C. Maurette M., Kurat G., Gounelle M. and Hammer C. 2007. Micrometeorites from central Antarctic snow: The CONCORDIA collection. *Advances in Space Research* 39:605-611.

Engrand C. E., McKeegan K. D., Leshin L. A., Herzog G. F., Schnabel C., Nyquist L. E. and Brownlee D. E. (2005) Isotopic compositions of oxygen, iron, chromium, and nickel in cosmic spherules: Toward a better comprehension of atmospheric entry heating effects. *Geochimica et Cosmochimica Acta* 69:5365-5385.

Feng H., Jones K. W., Tomov S., Stewart B., Herzog G. F., Schnabel C. and Brownlee D. E. 2005. Internal structure of type I deep-sea spherules by X-ray computed microtomography. *Meteoritics and Planetary Science* 40:195-206.

Friedrich J.M., Wignarajah D. P., Chaudhary S., Rivers M. L., Nehru C. E., Ebel D. S. 2008. Three-dimensional petrography of metal phases in equilibrated L chondrites. Effects of shock loading and dynamic compaction. *Earth Planet. Sci. Lett.* 275: 172-180.

Genge M. J., Grady M. M., and Hutchison R. 1997. The textures and compositions of fine-grained Antarctic micrometeorites - Implications for comparisons with meteorites. *Geochimica et Cosmochimica Acta* 61:5149-5162.

Genge M. J. and Grady M. M. 1998. Melted micrometeorites from Antarctic ice with evidence for the separation of immiscible Fe-Ni-S liquids during entry heating. *Meteoritics and Planetary Science* 33: 425-434.

Genge M. J. 2006. Igneous rims on micrometeorites. *Geochimica et Cosmochimica Acta* 70:2603-2621.

Genge M. J. 2008. Koronis asteroid dust in Antarctic ice. *Geology* 36:687-690.

Genge M. J., Engrand C., Gounelle M., and Taylor S. 2008. The classification of micrometeorites. *Meteoritics and Planetary Science* 43:497-515.

Goursat A. G. and Smeltzer W. W. 1973. Kinetics and morphological development of the oxide scale on iron at high temperatures in oxygen at low pressure. *Oxidation of metals* 6:101-116.

Heck P. R., Scmitz B., Baur H., and Wieler R. 2008. Noble gases in fossil micrometeorites and meteorites from 470 Myr old sediments from southern Sweden, and new evidence for the L-chondrite parent body break-up event. *Meteoritics and Planetary Science* 43:517-528.

Herzog G. F., Xue S., Hall G. S., Nyquist L. E., Shih C. Y., Wiesmann H., and Brownlee D. E. 1999. Isotopic and elemental composition of iron, nickel and chromium in type I deep-sea spherules: implications for origin and composition of the parent micrometeoroids. *Geochimica et Cosmochimica Acta*, 63, 1443-1457.

Jarosewich E. 1990. Chemical analyses of meteorites: A compilation of stony and iron meteorite analyses. *Meteoritics* 25:323-337.

Kimura M., Grossman J. N., and Weisberg M. K. 2011. Fe-Ni metal and sulfide grains in CM chondrites: An indicator for thermal history. *Meteoritics and Planetary Science* 46: 431-442.

Kurat G., Koeberl C., Presper T., Brandstatter F. and Maurette M. 1994. Petrology and geochemistry of Antarctic micrometeorites. *Geochimica et Cosmochimica Acta* 58:3879-3904.

Kurat G., Hoppe P., and Engrand C. 1996. A chondrule micrometeorite from Antarctica with vapor-fractionated trace element abundances. *Meteoritics and Planetary Science* 31: A75.

Love S. G. and Brownlee D. E. 1991. Heating and thermal transformation of micrometeoroids entering the Earth's atmosphere. *Icarus* 89:26-43.

Love S.G. and Brownlee D. E. 1993. A direct measurement of the terrestrial mass accretion rate of cosmic dust. *Science* 262: 550- 553.

Love S. G. and Brownlee D. E. 1994. Peak atmospheric entry temperatures of micrometeorites. *Meteoritics* 29:69-70.

Maurette M., Jehanno C., Robin E. and Hammer C. 1987. Characteristics and mass distribution of extraterrestrial dust from the Greenland ice cap. *Nature* 328:699-702.

Maurette M., Olinger C., Michel-Levy M. C., Kurat G., Pourchet M., Brandstatter F., and Bourot-Denise M. 1991. A collection of diverse micrometeorites recovered from 100 tonnes of Antarctic blue ice. *Nature* 351:44-47.

Millot F., Rifflet J. C., Wille G., and Saru-Kanian C. 2009. Density and surface tension of liquid iron oxides. *High Temperatures-High Pressures* 38:245-257.

Nesvorny D., Jenniskens P., Levison H. F., Bottke W. F., Vokrouhlicky D., and Gounelle M. 2010. Cometary origin of the zodiacal cloud and carbonaceous micrometeorites. Implications for hot debris disks. *The Astrophysical Journal* 713:826-836.

Noguchi R., Ohashi N., Tsujimoto S., Takuya M., Mitsunari T., Bradley J. P., Nakamura T., Shoichio T., Stephan T., Naoyoshi I., and Naoya I. 2015. Cometary dust in Antarctic ice and snow: Past and present chondritic porous micrometeorites preserved on the Earth's surface. *Earth Planet. Sci. Lett.* 410: 1-11.

Parashar K., Prasad M. S., and Chauhan S. S. S. 2010. Investigations on a large collection of cosmic dust from the central Indian Ocean. *Earth Moon and Planets* 107:197-217.

Rietmeijer F. J. M. 1998. Interplanetary dust particles. In *Planetary Materials*, Vol. 36, edited by J. J. Papike, Mineralogical Society of America. pp 28-119.

Rochette P., Folco L., Suavet C., van Ginneken M., Gattacceca J., Perchiazzi N., Braucher R. and Harvey R. P. 2008. Micrometeorites from the Transantarctic Mountains. *Proceedings of the National Academy of Sciences* 105: 18206-18211.

Rosen M. J. 2004. *Surfactants and interfacial phenomena*. Wiley. 443 p.

Rudraswami N. G., Parashar K. and Shyam Prasad M. 2011. Micrometer- and nanometer-sized platinum group nuggets in micrometeorites from deep-sea sediments of the Indian Ocean. *Meteoritics and Planetary Science* 46: 470-491.

Suavet C., Rochette P., Kars M., Gattacceca J., Folco L. and Harvey R. P. 2009. Statistical properties of the Transantarctic Mountains (TAM) micrometeorite collection. *Polar Science* 3:100-109.

Taylor S. and Brownlee D. E. 1991. Cosmic spherules in the geological record. *Meteoritics* 26:203-211.

Taylor S., Lever J. H., and Harvey R. P. 2000. Numbers, types and compositions of an unbiased collection of cosmic spherules. *Meteoritics and Planetary Science* 55:651-666.

Taylor S., Matrajt G., Lever J. H., Joswiak D. J. and Brownlee D. E. 2007. Size distribution of Antarctic micrometeorites. Proc. 'Dust in Planetary Systems', Kauai, Hawaii, USA. 26--30 September 2005 (ESA SP-643, January 2007).

Vondrak T., Plane J. M. C., Broadley S., and Janches D. 2008. A chemical model of meteoric ablation. *Atmospheric Chemistry and Physics* 8:7015-1031.

Wang J., Davis A. M., Clayton R. N., and Mayeda T. K. 1994. Kinetic isotopic fractionation during the evaporation of the iron oxide from liquid state. 25th Lunar and Planetary Science Conference. pp. 1459–1460.

Weisberg M. K., Prinz M., Clayton R. N. and Mayeda T. K. 1993. The CR(Renazzo-type) carbonaceous chondrite group and its implications. *Geochimica et Cosmochimica Acta* 57:1567-1586.

Xue S., Herzog G. F., Hall G. S., Bi D. and Brownlee D. E. 1995. Nickel isotope abundance of type I deep-sea spherules and of iron-nickel spherules from sediments in Alberta, Canada. *Geochimica et Cosmochimica Acta* 59:4975-4981.

Yada T., Sekiya M., Nakamura T. and Takaoka N. 1996. Numerical simulation of I-type spherule formation. *Lunar and Planetary Science* 27: 1463.

Young D. 2008. High temperature oxidation and corrosion of metals. Elsevier, Amsterdam. 574 p.

Zhang H., Vardelle A. and Themelis N. J. 2003. In-flight oxidation and evaporation of plasma-sprayed iron particles. *High Temperature Materials Processes* 7, 277-298.

Zolensky M. E. , Zega T. J., Yano H., Wirick S., Westphal A. J., Weisberg M. K., Weber I., Warren J. L., Velbel M. A., Tsuchiyama A., Tsou P., Toppani A., Tomioka N., Tomeoka K., Teslich N., Taheri M., Susini J., Stroud R., Stephan T., Stadermann F. J., Snead C. J., Simon S. B., Simionovici A., See T. H., Robert F., Rietmeijer F. J., Rao W., Perronnet M. C., Papanastassiou D. A., Okudaira K., Ohsumi K., Ohnishi I., Nakamura-Messenger K., Nakamura T., Mostefaoui S., Mikouchi T., Meibom A., Matrajt G., Marcus M. A., Leroux H., Lemelle L., Le L., Lanzirotti A., Langenhorst F., Krot A. N., Keller L. P., Kearsley A. T., Joswiak D., Jacob D., Ishii H., Harvey R., Hagiya K., Grossman L., Grossman J. N., Graham G. A., Gounelle M., Gillet P., Genge M. J., Flynn G., Ferroir T., Fallon S., Fakra S., Ebel D. S., Dai Z. R., Cordier P., Clark B., Chi M., Butterworth A. L., Brownlee D. E., Bridges J. C., Brennan S., Brearley A., Bradley J.P., Bleuet P., Bland P. A. and Bastien R. 2006. Mineralogy and petrology of comet 81P/Wild 2 nucleus samples. *Science* 314:1735-1739.

Figure Captions

Figure 1. Showing scanning electron images of Antarctic I-type spherules. (a) A backscattered electron image (BEI) of CP91-050-118 showing dendritic wustite crystals forming a granular texture. (b) A BEI of CP94-100-023 showing fine-grained iron oxides with an irregular central void. (c) A BEI of SP009, 5-A92 exhibiting an iron oxide mantle surrounding a subordinate, off-centre, Fe-Ni metal bead. (d) A BEI of SP009, 5-B91 exhibiting a Fe-Ni metal bead at the margin of the oxide sphere. A thin meniscus of iron oxide covers the exterior of the metal bead. (e) A secondary electron image (SEI) of CP91-050-118 showing a protrusion on the surface of the particle. (f) A SEI of CP91-050-129 showing equant crystals on the exterior and a cavity surrounded by a surface deposit of oxide. Spherule with particle numbers beginning CP were collected by Maurette and coworkers (Maurette et al., 1991) by melting and filtering of Antarctic blue ice. Spherules with SP particle numbers were collected by from the South Pole Water Well and images were provided courtesy of Susan Taylor (Taylor et al., 2000).

Figure 2. The phase diagram for Fe-O (Darken, 1946).

Figure 3. Showing the temperature and radii of silicate, iron metal only, iron oxide only and oxidizing iron micrometeoroids.

Figure 4. Showing the variation of peak temperature (K) of silicate and oxidizing iron micrometeoroids with radii, entry angle and velocity. The shaded regions show particles that decelerate without melting.

Figure 5. The duration of heating above the solidus for silicate and oxidizing iron micrometeoroids in seconds.

Figure 6. Showing the altitudes (km) at which oxidizing iron micrometeoroids attain peak temperature.

Figure 7. Showing the ratio of final radii to initial radii of silicate and oxidizing iron micrometeoroids.

Figure 8. Showing time-radii profiles for oxidizing iron micrometeoroids under different entry parameters.

Figure 9. Showing the mass proportion of iron metal beads within simulated oxidizing iron particles.

Figures are provided separately

Table 1. Symbols used in equations.

Symbol	Value
v	Velocity
r	Particle radius
g	Gravitational acceleration 9.80665 m s^{-1}
ρ_m	Particle density
ρ_a	Atmospheric density
ρ_o	Atmospheric oxygen density
m	Particle mass
L_v	Latent heat of evaporation
σ	Stefan Boltzman constant
ε	Emissivity (assumed 1.0)
q	Heat
T	Temperature
t	Time
A, B	Parameters of the Langmuir Equation
p_v	Vapor pressure
m_{mol}	Average molecular mass of vapor
γ	Surface transfer constant for oxygen
ΔH_{ox}	Heat of oxidation of iron metal

Figure 1

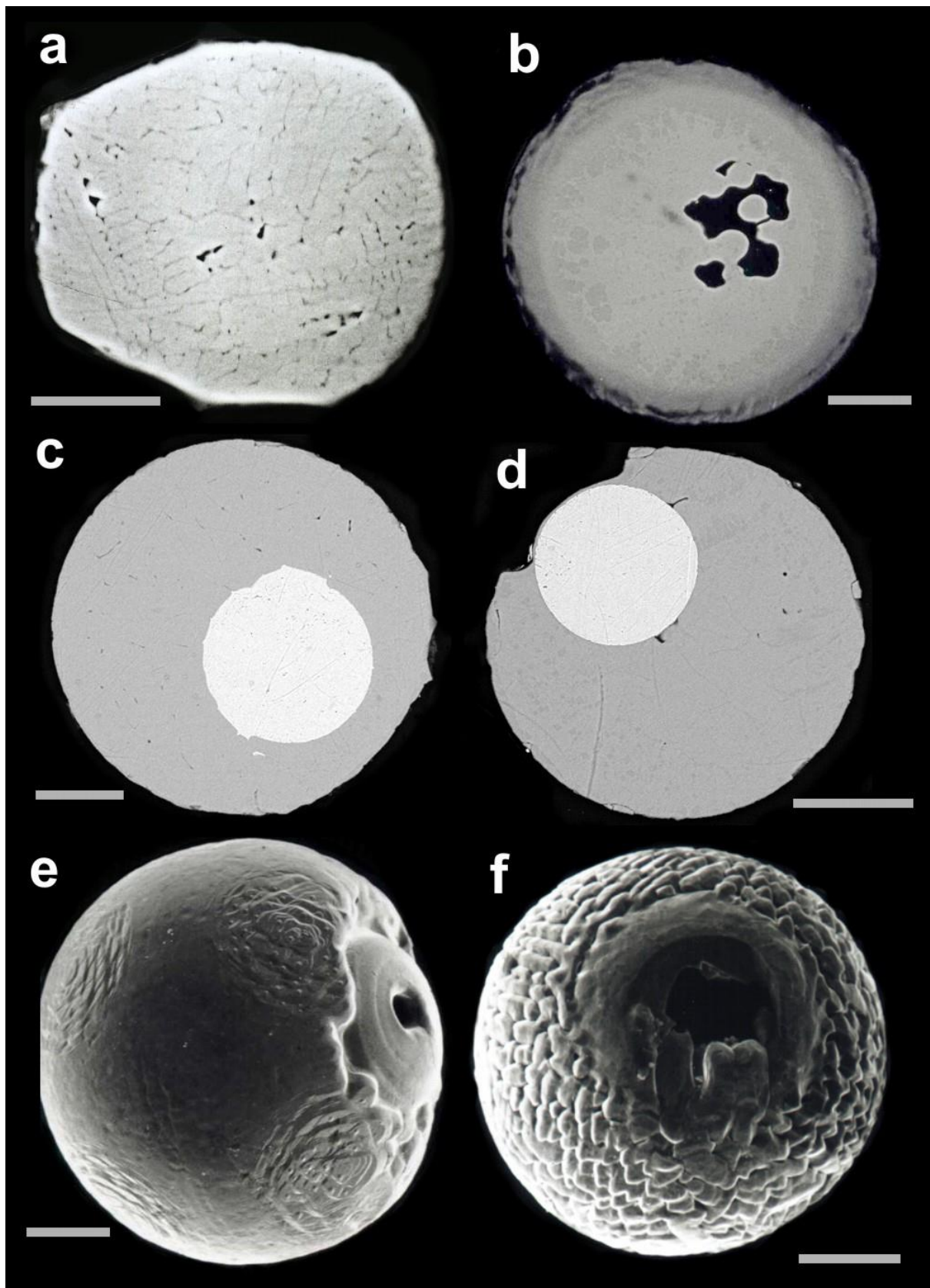


Figure 2

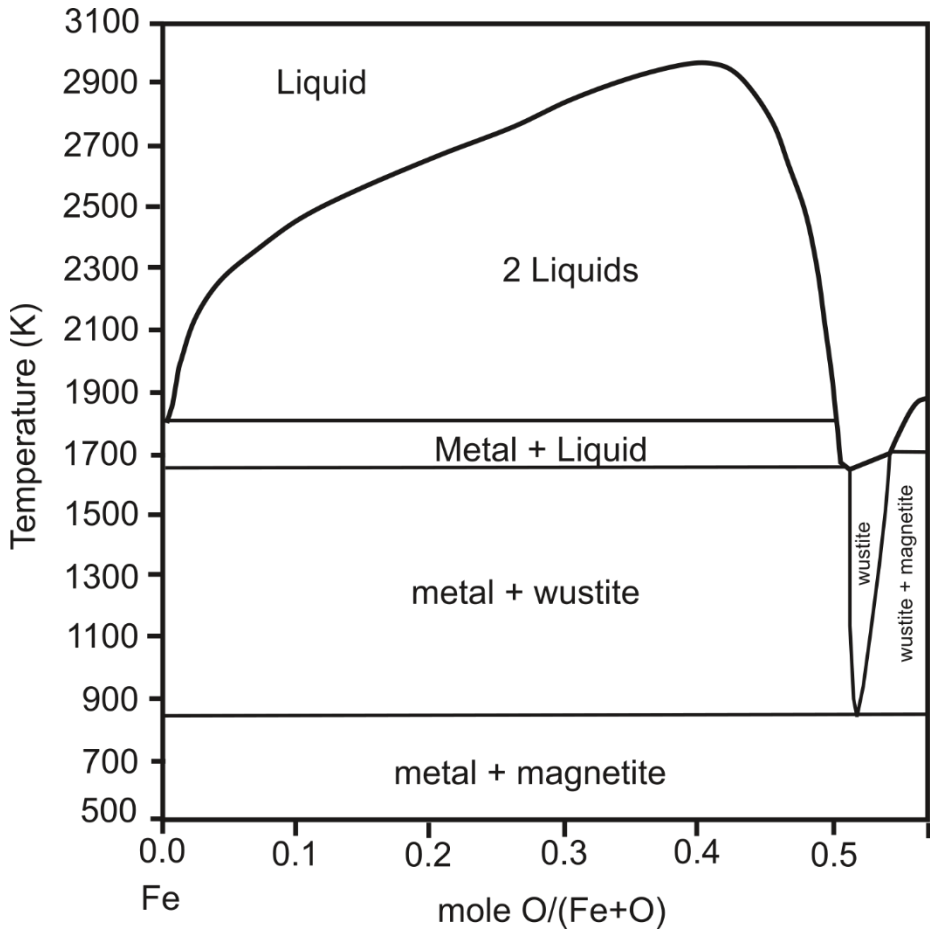


Figure 3

Figure 3

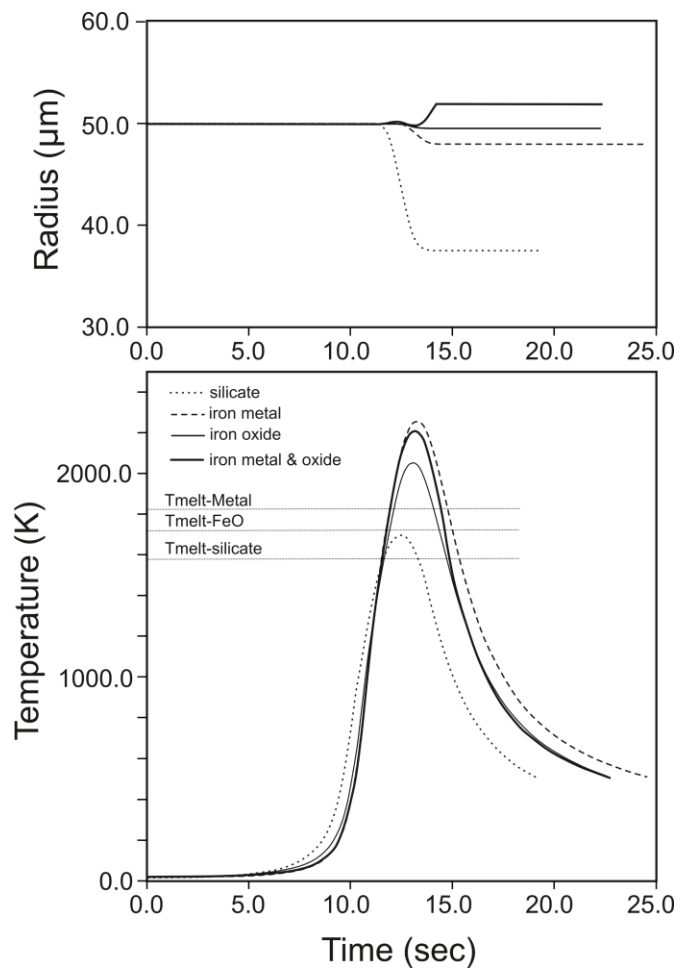


Figure 4

Figure 4

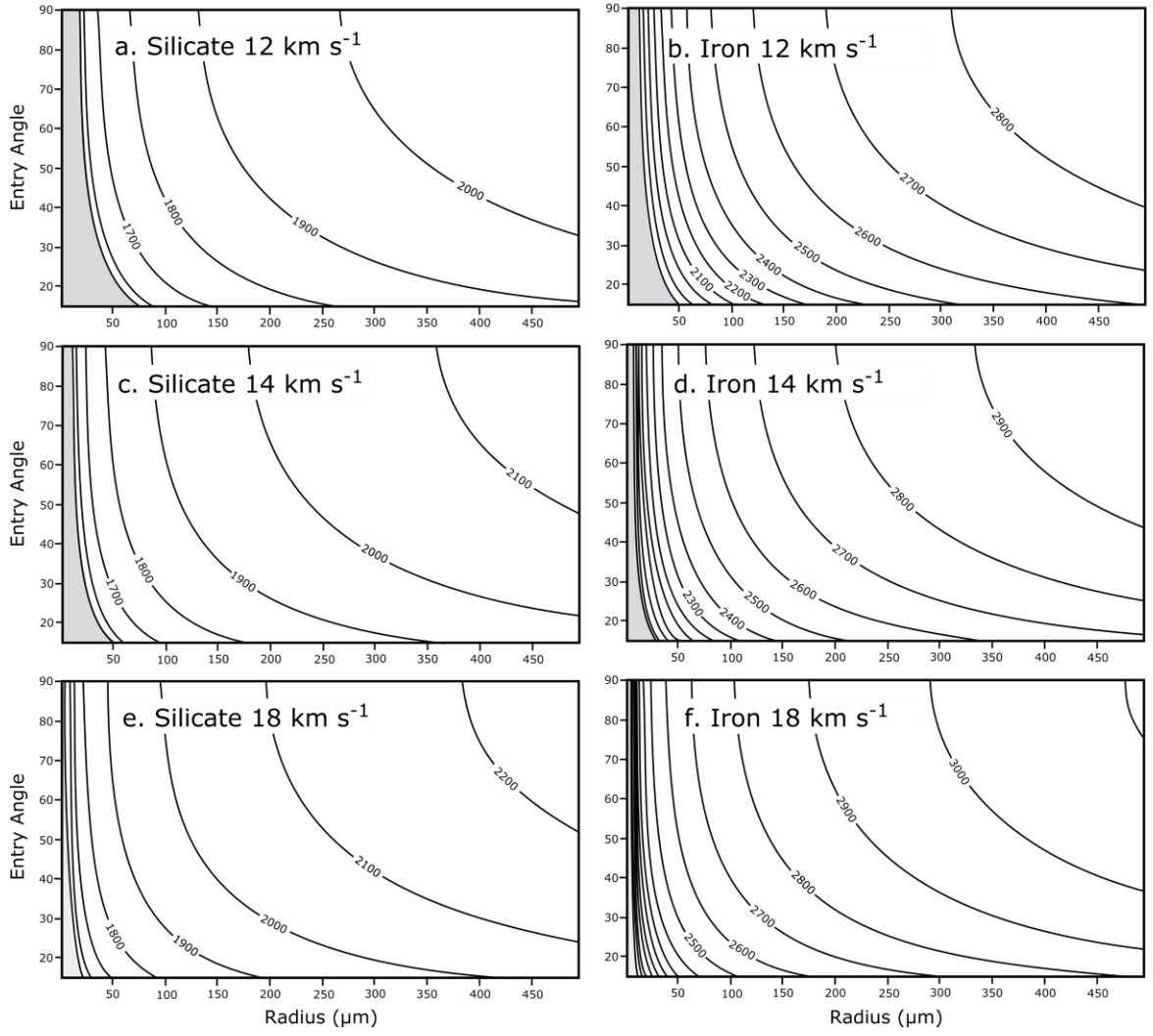


Figure 5

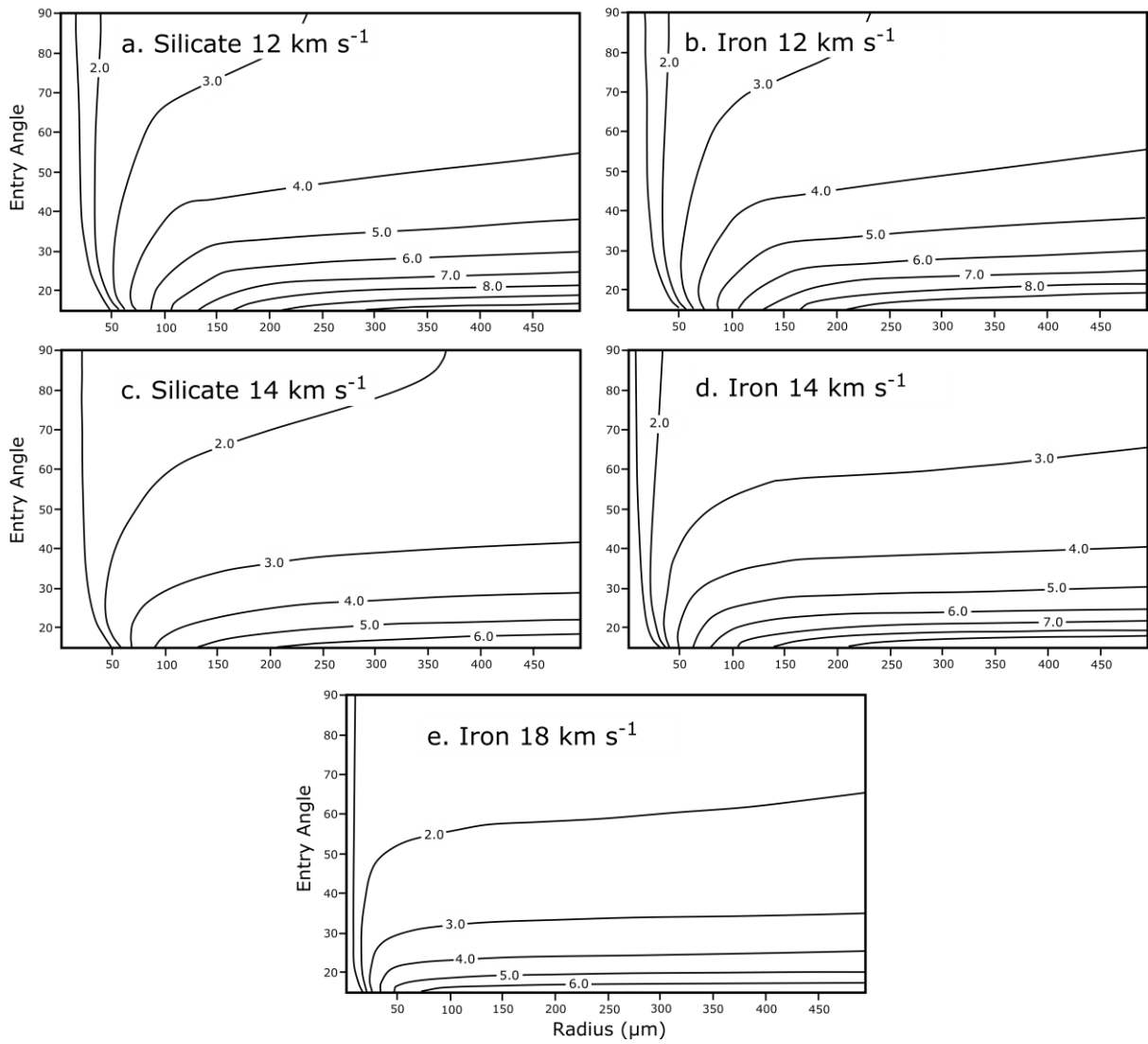


Figure 6

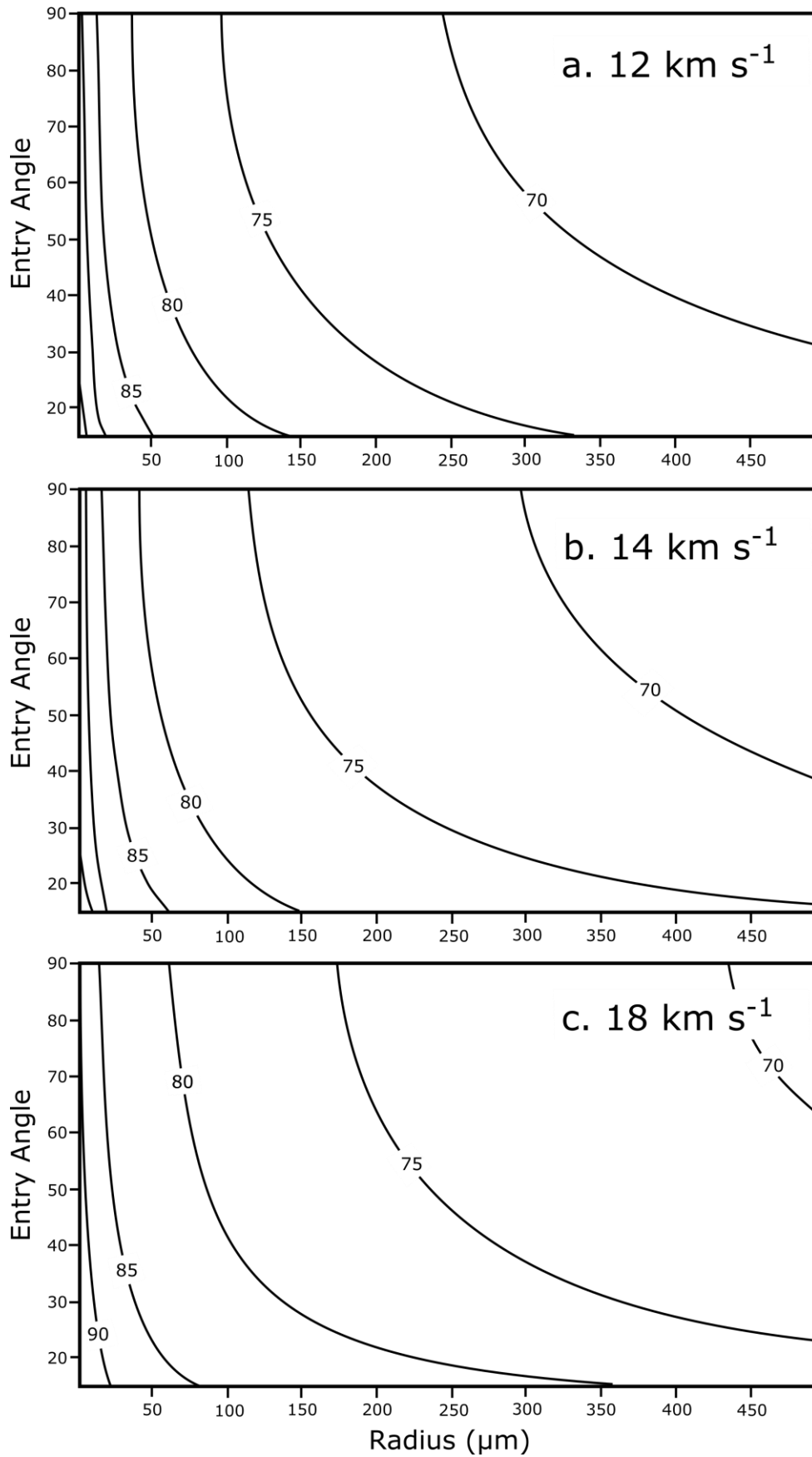


Figure 7

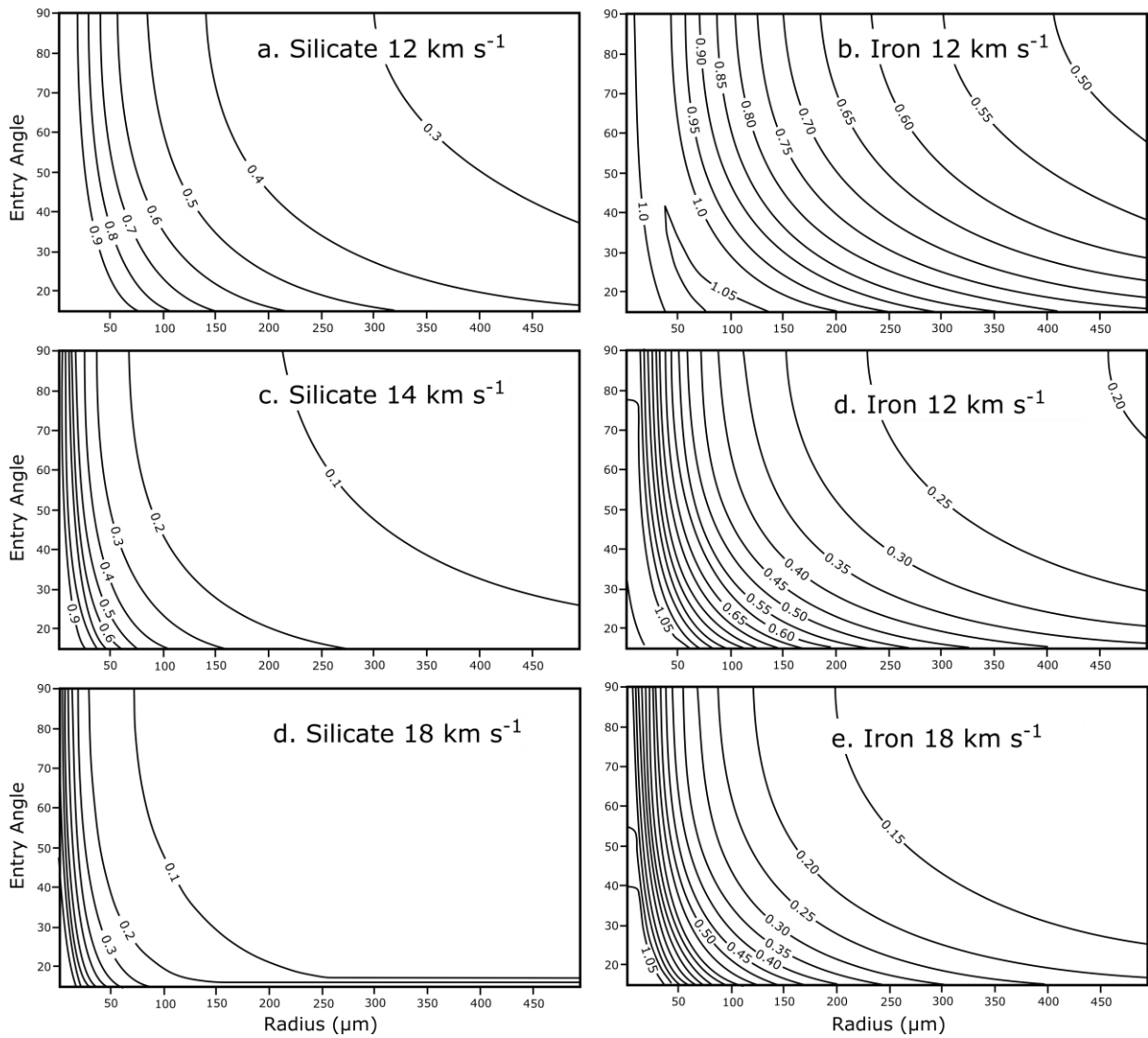


Figure 8

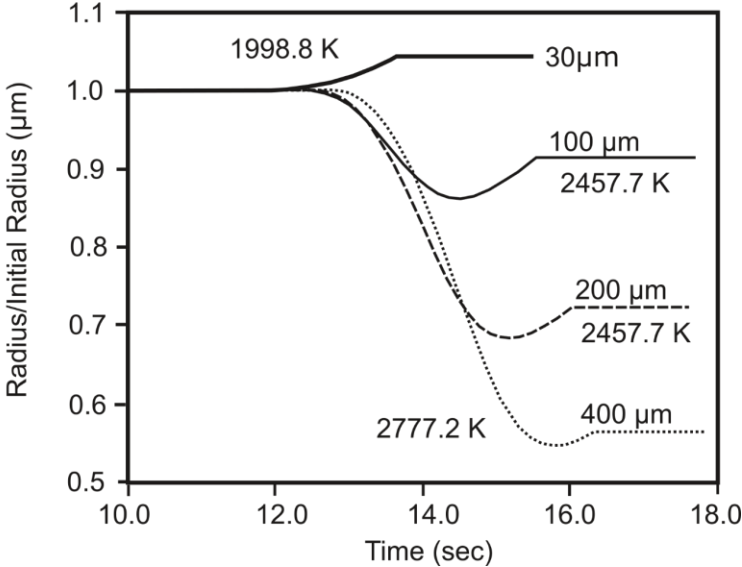
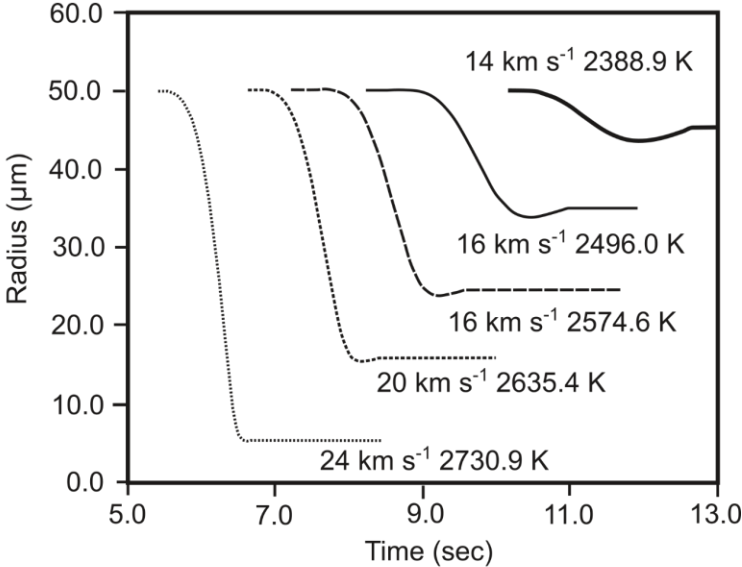
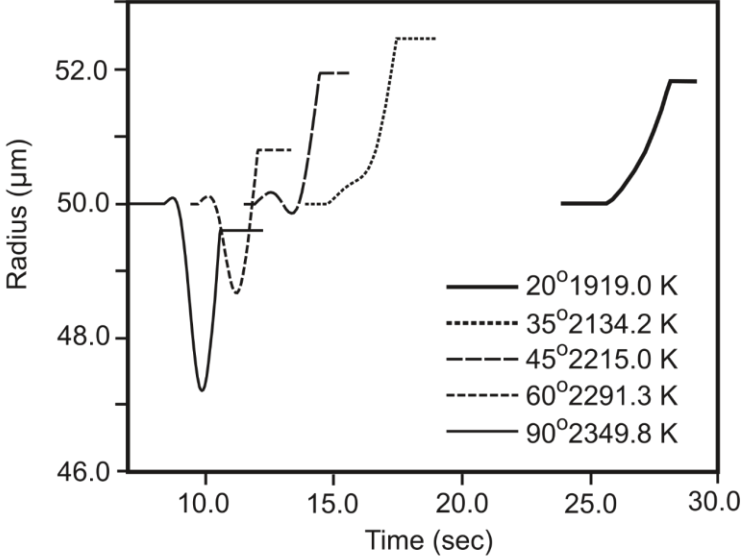


Figure 9

